RUNE JOHNSON

AN EXAMINATION OF SOME STRUCTURE IN THE PHONON DISPERSION CURVES FOR ALUMINIUM

Synopsis

Some observed structure in the phonon dispersion curves in the [111]-direction in Al is compared with theoretical calculations in a local potential approximation of the interaction between the ions and the conduction electrons. A previously derived expression for the lowest order non-diagonal part of the R.P.A. dielectric matrix is shown to account for most of the structure. The same approximation of the imaginary part of the dielectric matrix is also shown to satisfactorily reproduce the observed phonon damping in the longitudinal mode.

The accuracy of the neutron spectroscopy is by now so high that it is possible to obtain very detailed phonon dispersion curves. It has then been shown that in many metals there are rather complicated strucures in these curves that may contain much information about the microscopic situation in the crystal [1], [2], [3], [4]. A closer analysis of this structure seems for that reason to be well worth while and in this short note we report some results of a comparison between some recent accurate experimental results (at $80°K$) [4] and a theoretical model previously used in phonon calculations [5], [6]. As an example we will here concentrate on only one symmetry direction and this only for small q (the phonon momentum), where the analysis is relatively simple. A more complete account of the subject will be given elsewhere.

The phonon frequencies $\omega_i(\boldsymbol{q})$ are in the harmonic approximation given of the three lowest eigenvalues to the dynamical matrix

$$\omega_i^2(\boldsymbol{q}) \cdot \boldsymbol{e}_i = \omega_p^2 D(\boldsymbol{q}, \omega) \cdot \boldsymbol{e}_i \tag{1}$$

where $\boldsymbol{e}_i$ is the phonon polarisation vector and $\omega_p (\simeq 18.91 \cdot 10^{13} \ r/s$ in Al at $80°K$) is the plasma frequency for the ions. In a metal the matrix D is naturally split into an ionic part D_i and an electronic part D_e, where in the local potential approximation of the unscreened ion-electron interaction the part D_e has the following form in a simple lattice

$$
\begin{aligned}
D_e(\boldsymbol{q}, \omega) = -\frac{1}{4\pi} \Bigg\{ &\sum_{\boldsymbol{K'}, \boldsymbol{K''}} \frac{v_e(\boldsymbol{K'} + \boldsymbol{q}) v_e(\boldsymbol{K''} + \boldsymbol{q})(\boldsymbol{K'} + \boldsymbol{q})(\boldsymbol{K''} + \boldsymbol{q})}{[v(\boldsymbol{K'} + \boldsymbol{q}) v(\boldsymbol{K''} + \boldsymbol{q})]^{1/2}} \cdot \\
&\cdot \langle \boldsymbol{K'} + \boldsymbol{q} | \frac{e^2 \varkappa(\omega)}{1 + e^2 \varkappa(\omega)} | \boldsymbol{K''} + \boldsymbol{q} \rangle \text{-similar terms with } q = \omega = 0 \Bigg\}
\end{aligned}
\tag{2}
$$

where $\boldsymbol{K}$ is a vector in the reciprocal lattice $v_e(\boldsymbol{k})$, $v(\boldsymbol{k})$ are the Fourier transforms of the ion-electron and electron-electron interactions (per unit charge square) and $1 + e^2 \varkappa(\omega)$ is the symmetrized dielectric matrix for the conduction electrons with the elements in Eq. (2) in a plane wave representation. It is the structure in the q-dependence of these elements that is reflected

in the dispersion curves. For a uniform conduction electron system the dielectric matrix is diagonal in the plane wave representation and in the R.P.A.-approximation its elements are given by the Lindhard formula. The structure in $D_e (= D_{e0}$ in that case) is then the structure pointed out by KOHN [7]. Inclusion of effects on the electron system from the periodic lattice potential gives a more general dielectric matrix containing also non-diagonal elements in the plane wave representation. In the R.P.A. approximation of $\varkappa$ calculations indicate [6] that its diagonal elements ($\boldsymbol{K}' = \boldsymbol{K}''$) are in the actual case (nearly free electrons) quite accurately given by the Lindhard formula whereas the non-diagonal elements ($\boldsymbol{K}' \neq \boldsymbol{K}''$), although much smaller than the diagonal elements, are considerable. With $\varkappa = \varkappa_0 + \varkappa_1$, where $\varkappa_0$ is the Lindhard matrix and $\varkappa_1$ is the important, purely non-diagonal correction to it, we can expand D_e in Eq. (2) and get to first order in $\varkappa_1$

$$D_e = D_{e0} + D_{e1} \tag{3}$$

where we expect D_{e1} to be responsible for much of the structure in the dispersion curves [5], [6]. This opinion is supported by some of the experimental results in that the same observed peak has different signs in different branches in the same direction. For the elements of $\varkappa_1$ the following lowest order expression was derived in [5]

$$e^2 \langle \boldsymbol{K}' + \boldsymbol{q} | \varkappa_1 | \boldsymbol{K}'' + \boldsymbol{q} \rangle = [v(\boldsymbol{K}' + \boldsymbol{q}) v(\boldsymbol{K}'' + \boldsymbol{q})]^{1/2} \frac{k_0}{\pi^2 a_0} \frac{V(\boldsymbol{K})}{\varepsilon_0} u_1(\boldsymbol{K}, \boldsymbol{K}' + \boldsymbol{q}) \left. \right\}$$
$$(\boldsymbol{K}' \neq \boldsymbol{K}'') \tag{4}$$

where $\boldsymbol{K} = \boldsymbol{K}'' - \boldsymbol{K}'$, $\varepsilon_0 = \dfrac{k_0^2}{2m}$ (≈ 0.867 Ry in Al) is the Fermi energy for the free electrons at $T = 0$ and $V(\boldsymbol{K})$ is the Fourier coefficient of the effective lattice potential for the electrons. $u_1(\boldsymbol{K}, \boldsymbol{q}')$ (where $\boldsymbol{q}' = \boldsymbol{K}' + \boldsymbol{q}$) is the first order function that was discussed in [5], [6] in the zero T and adiabatic ($\omega = 0$) limit.

$$u_1(\boldsymbol{K}, \boldsymbol{q}) = \frac{1}{8 Z_0 Z_1 s_1^2} \left\{ 2(Z_0 + c_1 Z_1) \ln \left| \frac{1 + Z_1}{1 - Z_1} \right| + \right.$$
$$+ 2(c_1 Z_0 + Z_1) \ln \left| \frac{1 + Z_0}{1 - Z_0} \right| - 2 c_1 Z_3 \ln \left| \frac{1 + Z_3}{1 - Z_3} \right| +$$
$$+ \mathrm{sgn}(R) \sqrt{R} [I(-Z_0, Z_1, c_1) - I(Z_1, Z_2, c_1) -$$
$$\left. - I(Z_0, Z_3, c_3) + I(Z_2, Z_3, c_3)] \right\} \tag{5}$$

where

$$Z_0 = \frac{|\boldsymbol{K}|}{2k_0}; \ Z_1 = \frac{|\boldsymbol{q}|}{2k_0}; \ Z_2 = Z_0 + 2c_1 Z_1$$

$$Z_3 = \frac{|\boldsymbol{K} + \boldsymbol{q}|}{2k_0}; \ c_1 = \frac{\boldsymbol{K} \cdot \boldsymbol{q}}{|\boldsymbol{K}||\boldsymbol{q}|}; \ s_1^2 = 1 - c_1^2$$

$$c_3 = \frac{Z_0 + c_1 Z_1}{Z_3}$$

and

$$I(a,b,c) = \begin{cases} \ln \left| \dfrac{c - ab - \sqrt{R(a,b,c)}}{c - ab + \sqrt{R(a,b,c)}} \right| & \text{if } R(a,b,c) > 0 \\[4mm] 2 \arctan \dfrac{c - ab}{\sqrt{R(a,b,c)}} & \text{if } R(a,b,c) < 0 \end{cases}$$

with

$$R(a,b,c) = a^2 + b^2 - 2abc - 1 + c^2; \ \sqrt{R(a,b,c)} = |R(a,b,c)|^{1/2}$$

and

$$R = R(-Z_0, Z_1, c_1)$$

Since the origin of u_1 is the first order effect from the lattice potential on the one-electron wave-functions but with still free particle one-electron energies it has a rather simple structure. It is axially symmetric about $\boldsymbol{K}$ and has a mirror plane in $2\boldsymbol{K} \cdot \boldsymbol{q}' + K^2 = 0$. Its derivative $\nabla_q u_1$ is logarithmically singular on the "Fermi spheres" $|\boldsymbol{q}'| = 2k_0$ and $|\boldsymbol{K} + \boldsymbol{q}'| = 2k_0$. More important in our case is, however, that for $|\boldsymbol{K}| < 2k_0$, $\nabla_q u_1$ is also singular on the shell where $(\boldsymbol{K} + \boldsymbol{q}')^2 - 4k^2 \sin^2 \theta = 0$ (θ is the angle between $\boldsymbol{K}$ and $\boldsymbol{q}'$), if $-K^2 \leqslant \boldsymbol{K} \cdot \boldsymbol{q}' \leqslant 0$. This singularity is stronger (of power $-1/2$) which is the reason why the effects from these terms are observable at all in spite of the small expansion parameter $\dfrac{V(\boldsymbol{K})}{\varepsilon_0}$ (a few per cent) in Eq. (4).

The geometry in the reciprocal space with an elementary cell laid in for an actual case is shown in Fig. 1, where $|\boldsymbol{K}'| = \sqrt{3}$, $|\boldsymbol{K}''| = 2$ and $|\boldsymbol{K}| = |\boldsymbol{K}'' - \boldsymbol{K}'| = \sqrt{3}$. $\boldsymbol{K}$ is in Fig. 1 the axis of symmetry in u_1 and the traces in the half-plane of the "Fermi spheres" around $0'$ and $0''$ are indicated. The trace of the shell with $(\boldsymbol{K} + \boldsymbol{q}')^2 - 4k_0 \cdot \sin^2 \theta = 0$ where $\nabla_q u_1$ is singular is also shown. It is a circle with radius k_0 and its centre at M on the mirror plane. The three points of intersection with this shell for an actual q in the [111] (or equivalent) direction are denoted by 1, 3 and 4 (a point 2 appears when $|\boldsymbol{K}'| = |\boldsymbol{K}''| = \sqrt{3}$ and $K = 2$). Two Kohn points in D_{e0} for
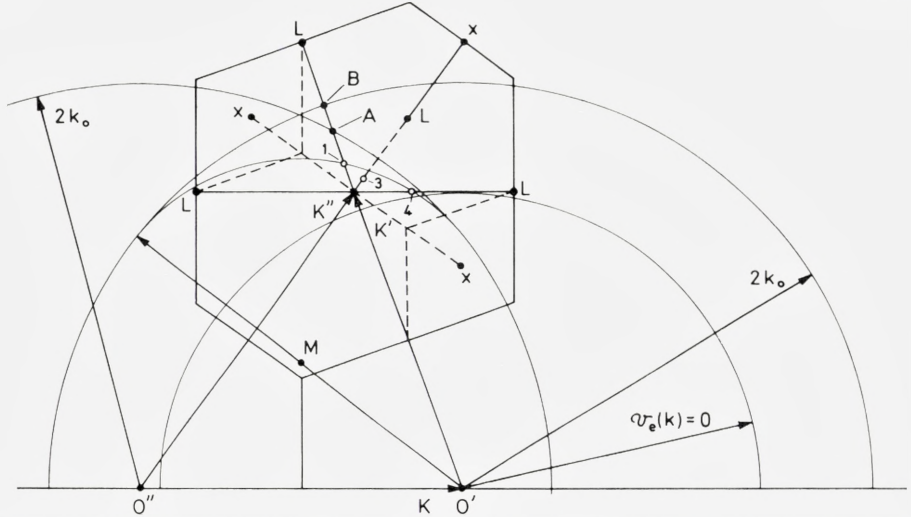
Fig. 1. The geometry in the reciprocal space showing a half-plane through the symmetry axis K in case $|K'| = \sqrt{3}$, $|K''| = 2$ and $|K| = \sqrt{3}$. Full lines are in the plane and dashed lines are out of the plane. The small open circles are some intersections with the shell $(K + q')^2 - 4k_0^2 \sin^2\theta = 0$ for a q in the [111] (or equivalent) direction. The dots A and B are the intersections with the "Fermi spheres" responsible for the Kohn anomalies in D_{e0} from these vectors (B from $K' = 1, 1, 1$ and A from $K' = 2, 0, 0$ or equivalent). For the explanation of the circle $v_e(k) = 0$, see the text.

this direction associated with the actual reciprocal lattice vectors are also denoted by A (one of three degenerate points) and B (non-degenerate). These four plus two points are the only critical points appearing in D_{e1} and D_{e0} for a q in the interval we are considering here. Some characteristics of the indicated critical points are collected in Table I.

In Fig. 2 we have collected results of a calculation of the contribution to the derivative $\dfrac{dD_e}{dq}$ from terms of interest. Curve a in 111L and the curve

TABLE 1.

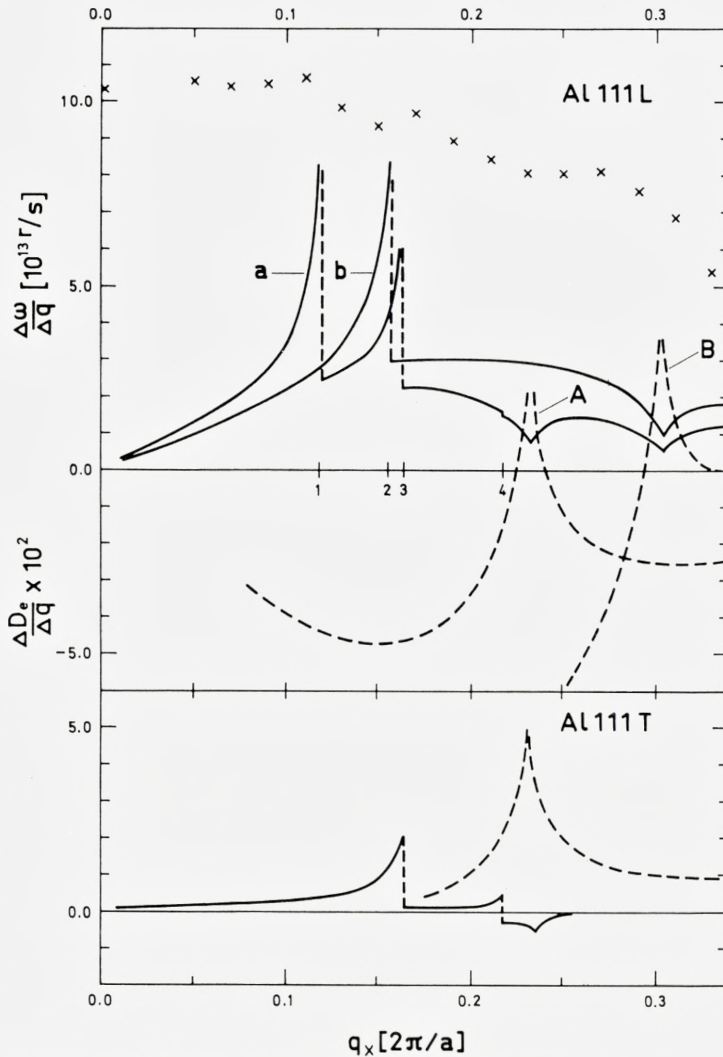| Point	q_x	Typical K'	Typical K''	$|K|$	Number of critical terms in D_e
1	0.119	1, 1, 1	2, 0, 0	$\sqrt{3}$	2×3
2	0.157	1, 1, 1	-1, 1, 1	2	2×3
3	0.164	1, 1, -1	2, 0, 0	$\sqrt{3}$	2×6
4	0.216	1, -1, -1	2, 0, 0	$\sqrt{3}$	2×3
A	0.231	2, 0, 0			3
B	0.302	1, 1, 1			1

Fig. 2. Contributions to $\frac{\Delta D_e}{\Delta q}$ from the terms discussed in the text. Curve a in 111L and the curve in full line in 111T give the contributions from non-diagonal terms in $\varkappa$ with $|K'| = \sqrt{3}, |K''| = 2$ (or vice versa) and $|K| = \sqrt{3}$ whereas curve b shows the contribution from terms with $|K'| = |K''| = \sqrt{3}$ and $|K| = 2$. The contributions from terms of interest in D_{e0} are also shown (dashed). In the figure are also the experimental $\frac{\Delta \omega}{\Delta q}$ shown in the longitudinal mode (marked as x) with the value for $q = 0$ from G. N. KAMM and G. A. ALERS, J. Appl. Phys. **35**, 327 (1964).

in full line 111T show the effects from the terms in D_{e1} of the type shown in Fig. 1 (i.e. $|\mathbf{K}'| = \sqrt{3}$, $|\mathbf{K}''| = 2$ or vice versa and $|\mathbf{K}| = \sqrt{3}$) and curve b in 111L shows the effects from terms with $|\mathbf{K}'| = |\mathbf{K}''| = \sqrt{3}$ and $|\mathbf{K}| = 2$. The latter terms give no particular effects in the transverse mode in the actual q-interval. In these calculations we have used the adiabatic and zero T function u_1 given in Eq. (5) and values on $V(\sqrt{3})$ and $V(2)$ given by ASHCROFT [8] (i.e. $V(\sqrt{3}) = -0.0179$ and $V(2) = -0.0562$ Ry), which seem to be the most reliable values available today. We have in Fig. 2 also shown (dashed) the contributions to $\dfrac{dD_{e0}}{dq}$ from terms in D_{e0} of interest (again in the adiabatic and zero T limit). Curve A shows the contribution from terms with $|\mathbf{K}'| = 2$, while the curve in 111T contains all vectors $|\mathbf{K}'| \leqslant 2$. The curve B, finally, shows the effect in $\dfrac{dD_{e0}}{dq}$ from the single term $\mathbf{K}' = (1,\,1,\,1)$, which explains why it is so oblique.

It is seen in Fig. 2 that the effects from the non-diagonal terms are quite comparable in size to those from D_{e0} although the terms themselves are much smaller. The reason for that is the earlier mentioned stronger singularity in $\nabla_q u_1$. The peak 4 is, however, rather weak in the transverse mode and almost invisible in the longitudinal mode due to a small factor $\mathbf{e}_L \cdot (\mathbf{K}' + \mathbf{q})$ there (can be seen in Fig. 1). We will comment on this exception later on.

In Fig. 2 we also observe a small effect from the logarithmic singularity in $\nabla_q u_1$ on the "Fermi spheres" in Fig. 1. Although small in the shown cases this is a significant effect, since it is present in many terms with for instance a fixed $\mathbf{K}'$ and different $\mathbf{K}''$. It turns out that in the actual cases the effects to the Kohn anomalies from D_{e0} is drastically reduced by these small but coherent contributions from the non-diagonal terms (can be seen in Fig. 12 in Ref. [6]). In particular the cancellation of the peak A is almost complete in the longitudinal mode, which explains why no visible peak is found there in the experimental $\dfrac{\Delta\omega}{\Delta q}$ shown in Fig. 2. This circumstance excludes the possibility of a simple determination of $v_e^2(2ko)$ by a comparison to the experimental results around the Kohn points.

A more detailed analysis of the experimental results is shown in Fig. 3. We show there the experimental quantity (q in $2\pi/a$)

$$d_{\exp}(q) = \frac{\omega_{\exp}^2(q)}{\omega_p^2 \cdot q^2} \tag{6}$$
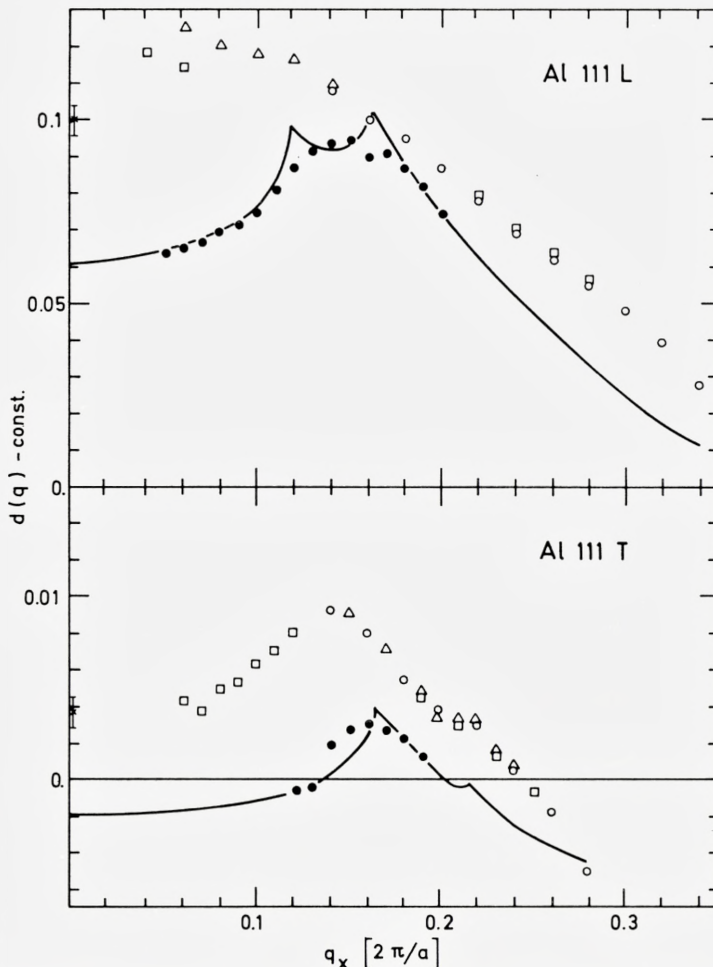
Fig. 3. $d_{exp} - c$ (width $c_L = 0.2$ and $c_T = 0.065$) and $d_{th} - c$ (with $c_L = 0.06$ and $c_T = 0.008$) versus q_x. The geometrical figures □ △ ○ indicate different experimental runs. The spread in the experimental values for different runs gives an idea of the accuracy. Experimental elastic values (with 1.5 per cent error bars) are from the reference in Fig. 2. The dots give theoretical values when the critical part in the analytic u_1 is replaced by a Monte Carlo sum.

which means that we determined (the real part of) the experimental eigenvalues of $D(q)$ by use of Eq. (1). These eigenvalues are in Eq. (6) divided by q^2 in order to get a more stable function in Fig. 3, where $d_{exp}(q)$ – const. (const. = 0.2 in the L-mode, = 0.065 in the T-mode) is plotted. The experimental curves are seen to contain interesting structures not present in D_{e0}. From D_i and D_{e0} in Eq. (1) we expect a d_{exp} which, as a function of q,

starts out rather constant or weakly increasing up to the broad humps just outside the Kohn points in D_{e0} after which the curve would rapidly decrease (can be qualitatively seen in Fig. 6 and Fig. 17 in [6]). However, as is seen in the figure, the experimental curves have quite different shapes. The rapid decrease starts much earlier and when compared to the theoretical curves also given in Fig. 3, the behaviour of the experimental and theoretical curves are seen to be very similar. Although the broad humps from the Kohn points in D_{e0} are visible in $d_{\exp}$ (at least in the longitudinal mode) they are much smaller than expected due to the earlier mentioned cancellations. In the theoretical curves shown in Fig. 3 we have calculated the (zero T and adiabatic) contribution to

$$d_{\text{th}}(q) = \frac{D_{e1}(q)}{q^2} \quad \left(q \text{ in } \frac{2\pi}{a} \right) \tag{7}$$

(and subtracted a const. = 0.06 in the L-mode, = 0.008 in the T-mode) where we in D_{e1} included only terms that give an appreciable structure in the actual q-interval (and keep the cubical symmetry of D_{e1}) i.e. the terms with $0 < |\boldsymbol{K'}|, |\boldsymbol{K''}|$ and $|\boldsymbol{K}| \leqslant 2$. A precise comparison between the theoretical and experimental curves in Fig. 3 is for that reason not possible, since we have to add to d_{th} a smooth function (out to the Kohn points in D_{e0}) in order to get the total d_{th}. This smooth function would, however, not alter the structure in the interesting q-interval.

Unfortunately, the experimental errors in the longitudinal mode increase so rapidly for decreasing q that the expected decrease in $d_{\exp}$ to the elastic limit [9] is not possible to establish, but in the transverse mode this effect is clearly seen. Anyway, the non-diagonal terms kept in d_{th} in the longitudinal mode here (only 72 out of about 10^4 almost equally important terms) give a surprisingly large contribution. (The situation is similar in the other symmetry directions.) So is for instance at $q = 0$ this contribution about 0.12 compared to the elastic value on $d_{\exp} \simeq 0.30$ with interesting implications to the elastic properties.

We have in Fig. 3 also given results (marked by dots) of a calculation where close to the critical point in the analytic u_1 we have replaced the critical contribution to the integral defining u_1 from the occupied electron states around the actual zone-plane by a Monte Carlo sum and in this sum used the correct one-particle energies (up to first order in the periodic potential). Details of this calculation will be given elsewhere.

The effect in the transverse mode from the critical point 4 is of particular

interest. Several experimental runs have established this effect (results of only two runs are shown in Fig. 3) and we have in fact used this peak when determining the function $v_e(k)$ used in these calculations. It turned out that the functions $v_e(k)$ used in earlier calculations [6] gave a (weak but) negative peak there. This was a consequence of the fact that the earlier functions had the first zero rather far out (at $k \simeq 1.7$). In order to remove this defect we had to adjust the first zero in $v_e(k)$ to a somewhat smaller value on k. This change made them almost identical with one of the functions used by VOSKO et al. [10]. Awaiting a direct experimental determination of the k-value where $v_e(k)$ is equal zero we have—so far—determined $v_e(k)$ by fitting our function $F(k)$

$$F(k) = \frac{1}{4\pi} \frac{v_e^2(k) k^2}{v(k)} \frac{e^2 \varkappa_0(k)}{1 + e^2 \varkappa_0(k)} \tag{8}$$

at $k = 2.5$ to the value of the corresponding function $F_0(k)$ in [10]. We think this can be of theoretical interest since their value at this point (they manipulate their values for smaller k) has a first principle calculation as a basis. The fit was made by simply adding a constant $\left(= -4\pi \cdot 0.03 \cdot \left(\frac{2\pi}{a}\right)^2\right)$ to a function $v_e(k)$ used in [6] (potential 3 there). In Fig. 4 we have compared the different functions $F(k)$ in the interval of interest ($1.6 < k < 2.25$). The zero in $v_e(k)$ is seen to be shifted from $k \simeq 1.7$ to $k \simeq 1.62$ by the adjustment. We have in Fig. 1 drawn the circle around $0'$ where the used $v_e(k)$ is zero and it is seen there how close the critical point 4 is to this circle.
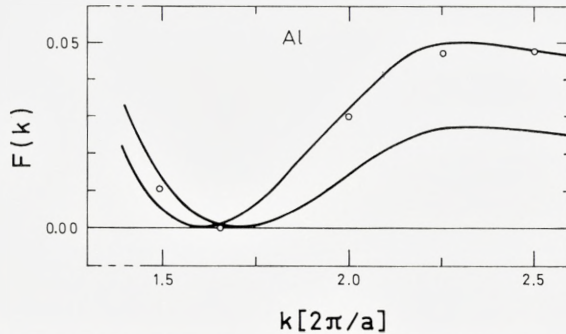

Fig. 4. The function $F(k)$ obtained with the potential $v_e(k)$ used in these calculations (upper curve at $k = 2.5$) compared to the function with a potential used in an earlier calculation. The small circles are estimated values from [10].
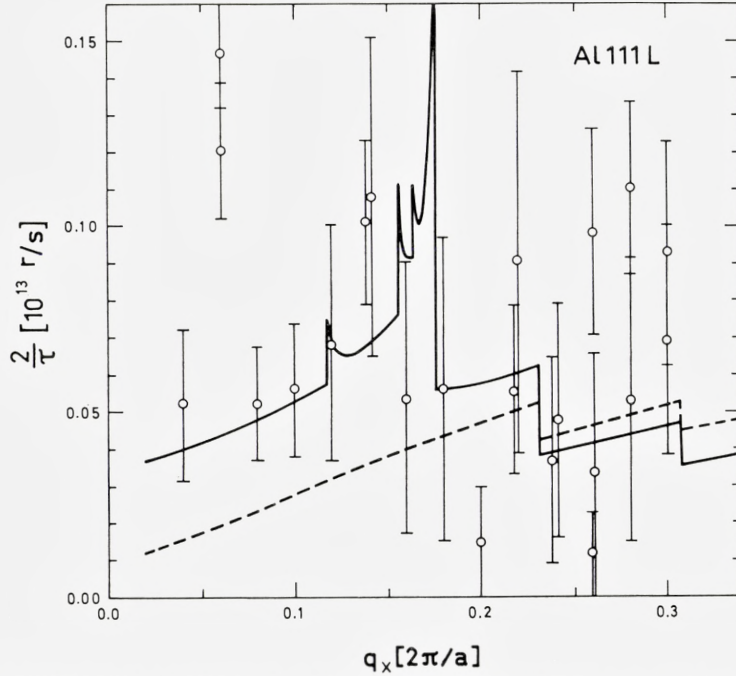
Fig. 5. Experimental and theoretical values for the phonon damping at small q in the 111L branch. In the theoretical curve only the electronic contribution is shown, but the anharmonic contribution is small for these q-values at this temperature $(80°\,K)$.

Finally, the new measurements have shown that the earlier reported experimental life-times τ at $80°K$ [11] for the phones in Al are somewhat too short. The new experimental results for small q in the 111L-mode in Al are shown in Fig. 5. The curves show the theoretical results when the function $v_e(k)$ and $V(K)$:s used in the other calculations here are put in the expression given in [12]. In the imaginary part of $\varkappa$ the non-diagonal terms included are again only those with $|\boldsymbol{K'}|,|\boldsymbol{K''}|$ and $|\boldsymbol{K}| \leqslant 2$, but here we have also included the important terms with $|\boldsymbol{K'}|$ or $|\boldsymbol{K''}| = 0$ $(|\boldsymbol{K}| \neq 0)$. The terms considered give in this case almost the entire contribution (the corrections from the remaining terms in $Im\varkappa$ are only of order a few per cent). The free electron part (dashed) is here, naturally, almost identical with the results given by Björkman et al. [13]. Considering the large uncertainties in both the experimental and theoretical results the agreement is seen to be remarkable good in this q interval, where the anharmonic contributions to the damping are small [14]. In particular there is some structure in the ob-

served results at the lower q end which we think might have observable effects on the temperature dependency of the resistance These effects on the resistance from the imaginary part of $\varkappa$ would correspond to the effects on the specific heat from the structure in the real part of $\varkappa$ [15].

I want to thank Dr. R. STEDMAN and Professor J. WEYMOUTH for making their experimental results available to me prior to their publication. My special thanks are due to Dr. R. STEDMAN for his patient answers to many questions about the experimental technique and difficulties.

References

[1] A. P. Miiller and B. N. Brockhouse, Phys. Rev. Letters **20**, 798 (1968).

[2] R. Stedman and G. Nilsson, Phys. Rev. Letters, **15**, 634 (1965).

[3] R. Stedman, L. Almqvist, G. Nilsson and G. Raunio, Phys. Rev. **162**, 545 (1967).

[4] R. Stedman and J. Weymouth (to be published).

[5] R. Johnson, Mat. Fys. Medd., Dan. Vid. Selsk. **37**, no. 9 (1970).

[6] R. Johnson and A. Westin, On phonons in simple metals II, AB Atomenergi, Stockholm, Sweden, Report AE-365 (1969).

[7] W. Kohn, Phys. Rev. Letters **2**, 393 (1959).

[8] N. W. Ashcroft, Phil. Mag. **8**, 2055 (1963).

[9] W. Gotze, Phys. Rev. **156**, 951 (1967).

[10] S. H. Vosko, R. Taylor and G. H. Keech, Can. J. Phys. **43**, 1187 (1965).

[11] R. Stedman and G. Nilsson, Phys. Rev. **145**, 492 (1965).

[12] R. Johnson, Electronic contributions to the phonon damping in metals, AB Atomenergi, Stockholm, Sweden, Report AE-328 (1968).

[13] G. Björkman, B. I. P. Lundqvist and A. Sjölander, Phys. Rev. **159**, 551 (1967).

[14] T. Högberg and R. Sandström, Physica Status Solidi, **33**, 169 (1969).

[15] R. Stedman, L. Almqvist and G. Nilsson, Phys. Rev. **162**, 549 (1967).